Supporting Information for

Photovoltage and photocurrent absorption spectra of sulfur vacancies locally patterned in monolayer MoS_2

Alexander Hötger[1], Wolfgang Männer[1], Tomer Amit[2], Daniel Hernangómez-Pérez[2],Takashi Taniguchi[3], Kenji Watanabe[4], Ursula Wurstbauer[5], Jonathan J. Finley[1], Sivan Refaely-Abramson[2], Christoph Kastl[1], Alexander W. Holleitner[1]

[1]Walter Schottky Institute and Physics Department, TU Munich, 85748 Garching, Germany
[2]Department of Molecular Chemistry and Materials Science, Weizmann Institute of Science, Rehovot, Israel
[3]Research Center for Materials Nanoarchitectonics, National Institute for Materials Science, 1-1 Namiki, Tsukuba 305-0044, Japan
[4]Research Center for Electronic and Optical Materials, National Institute for Materials Science, 1-1 Namiki, Tsukuba 305-0044, Japan
[5]Institute of Physics, Westfälische Wilhelms-Universität Münster, 48149 Münster, Germany

S1: Fabrication. We mechanically exfoliate monolayer MoS_2, graphene and hexagonal boron nitride hBN flakes using scotch tape from bulk crystals. We use MoS_2 crystals from HQgraphene, graphite crystals from NGS, and high quality synthesized hBN crystals. Suitable flakes are transferred via dry visco-elastic stamping on top of each other, to build a van-der-Waals heterostack. As substrate we use Si wafer with a 285 nm thick tempered SiO_2 layer. Before assembly we evaporate 20 nm thick gold contacts on the substrate with a 5 nm thick titanium adhesion layer. After assembly we anneal the sample at 150 °C for 1h in Ar/H_2 (95:5) atmosphere. The focused He-ion irradiation was performed with an acceleration voltage of 30 keV. The irradiated pattern are circular patches with 400 nm diameter arranged in an array pattern with a pitch of 2 µm. The irradiated patches consist of several dwell points with a pitch of 5. For each irradiated region, the irradiation dose can then be expressed as

$$dose = \frac{beam\ current \times dwell\ time}{effective\ area}.$$

It is evident that a small beam current and dwell time will result in a low dose. However, the noise level of the beam current readout is at 1 pA, which sets, together with the lowest possible dwell time of 0.1 µs per dwell point, a lower limit for the dose. By using the minimum achievable beam current of 1 pA, a dwell time of 5 µs and an effective area of 5 nm in diameter (pitch between dwell points), the dose can be calculated to ~ 2.4 µC cm^{-2} (~ $1.5 \cdot 10^{13}$ ions cm^{-2}).

S2: Experimental details. The optical measurements are taken in a home-build confocal microscope. The sample is mounted in a He-flow cryostat and a vacuum of 10^{-6} mbar. The light of a tunable laser source is focused onto the sample with a 50x objective (NA = 0.42). The spectral bandwidth of the tunable excitation laser is <2.5 nm. For the photoluminescence measurements, a

long pass filter (600 nm cut-off wavelength) is blocking the laser beam in front of the spectrograph. For the photocurrent spectroscopy measurements, we keep the power at a constant value per wavelength through a feedback loop. After amplification in a current-voltage amplifier, we measure the photocurrent I_{Photo} in a lock-in amplifier. We modulate the laser excitation with a chopper wheel at a frequency of 966 Hz, which is fed to the lock-in amplifier as reference signal. All photocurrent results presented in the main manuscript are recorded in this configuration, except for the results shown in Fig. 3 and Figs. 4a,b. For the data in Fig. 3, we measure the signal of the open-circuit measurements with a digital multimeter connected directly after the current-voltage amplifier, without the modulation of the laser by a chopper and without the use of a lock-in amplifier. The time-resolved data as shown in Figs. 4a,c are recorded by the help of an oscilloscope. Here, we feed the signal of the current-voltage amplifier into one port of the oscilloscope and use the reference frequency of the laser chopper as a trigger signal. We calculate the photocurrent responsivity by dividing the measured photocurrent I_{Photo} by the laser power at each specific wavelength.

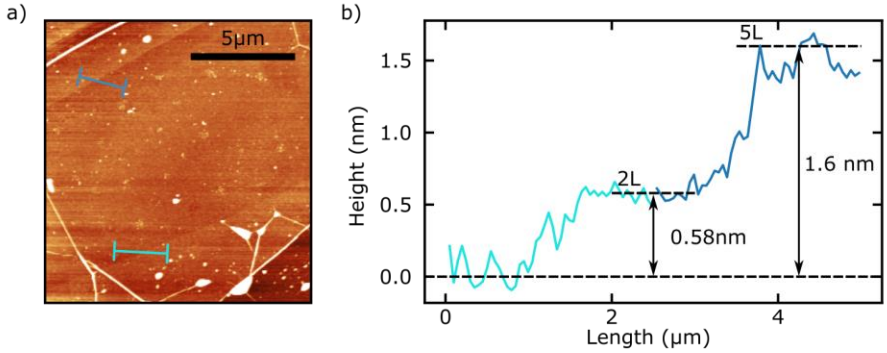

Figure S1: Atomic force microscope (AFM) measurements on the thickness of the utilized hBN barrier. a) AFM images of the hBN tunneling barrier before being stacked to act as a tunneling barrier in the heterostructure, as shown in the main manuscript. Scale bar is 5µm. b) Height profiles of the hBN tunneling barrier marked in a) showing a region with height 0.58 nm, which is equivalent to bilayer of hBN, and a region of 1.6 nm (quintuple layer).

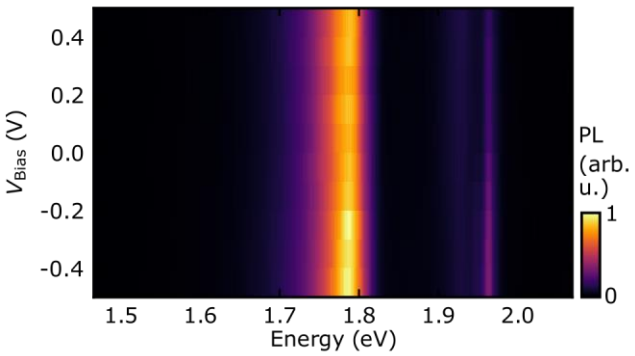

Figure S2: Bias-voltage-dependent photoluminescence spectra. Photoluminescence spectra measured at a defect site on the sample, as discussed in the main manuscript, versus the applied bias voltage V_{Bias} at 10 K. Within the applied bias range, no significant indication of doping could be resolved. Together with an increasing dark current (Fig. S3), this suggests that charge carrier tunnel instead of getting accumulated. For devices with a thicker hBN barrier (cf. Fig. S4), the accumulation is more likely and in turn, the increasing Fermi level results in the occupation of the defect states *c*D1 and *c*D2 which is observed by a quenching of the defect photoluminescence.

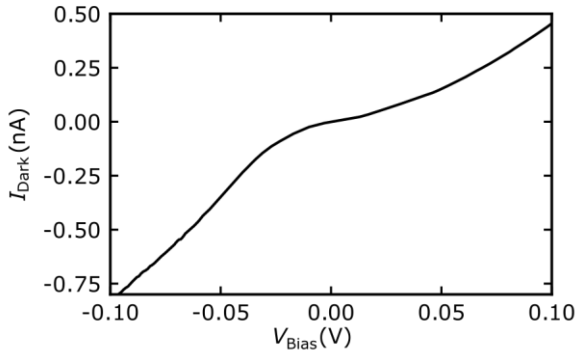

Figure S3: Low-temperature dark current curve. I_{Dark} versus V_{Bias} curve at 10 K.

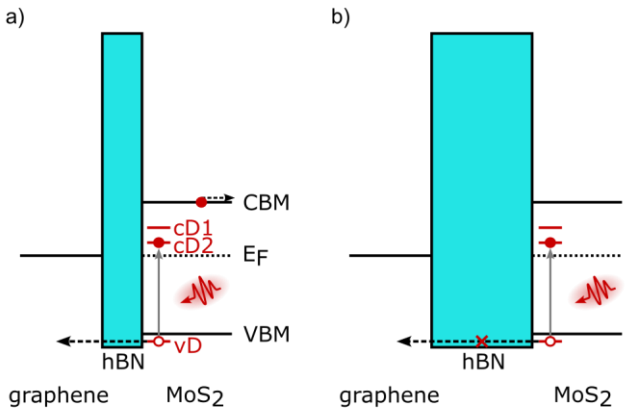

Figure S4: Schematic band diagram of devices with different hBN barriers. a) A thin hBN barrier results in a direct tunneling of holes through the insulating barrier. b) A thicker hBN barrier greatly reduces the hole tunneling.

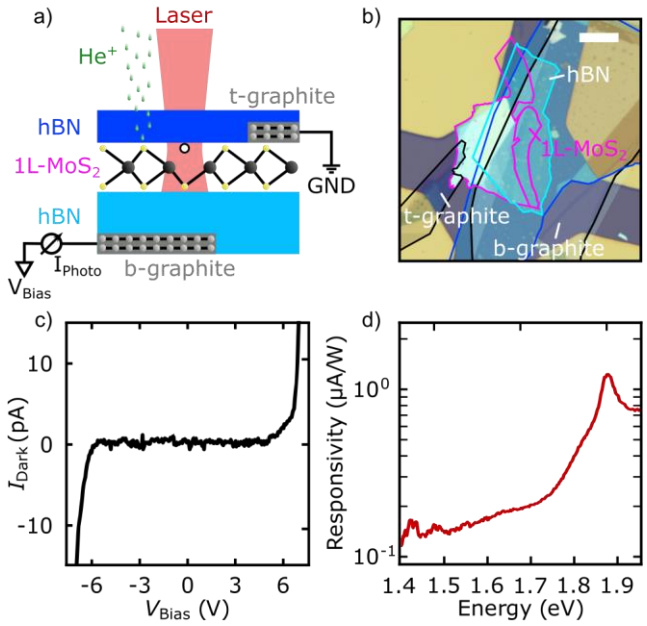

Figure S5: Characterization of a second sample. a) Sketch of heterostack of second sample. b) Optical microscope image of the heterostack. Scale bar is 10 µm. c) Dark-current I_{Dark} (i.e. without laser exciation) vs bias voltage V_{Bias}. d) Photocurrent responsivity spectrum at the position of a defect site at room temperature.

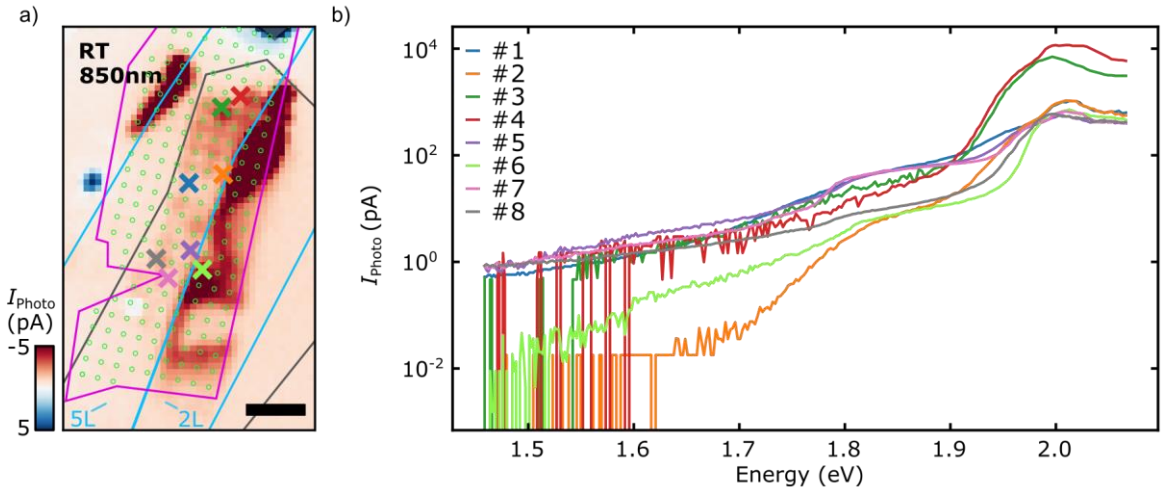

Figure S6: Statistics on photocurrent spectra. a) Photocurrent map with a laser excitation of 850 nm (1.46 eV) at room temperature. Scale bar is 5 µm. b) Low temperature photocurrent spectra at eight positions. The individual PC spectra are measured at the crosses with the corresponding color in a). We note that there are certain mutual position uncertainties, ie. during HIM-exposure e.g. by charging effects, and positioning of the excitation laser, while the photon energy is swept and the bath temperature is kept constant. Still, in all photocurrent spectra measured at the exposure sites, a sub-bandgap photocurrent shows up.

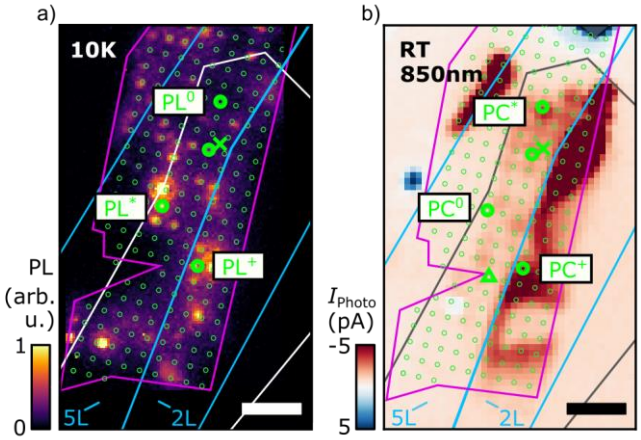

Figure S7: Comparison of photocurrent and photoluminescence signals. a) Low temperature PL map with marked positions PL^0, PL^*, and PL^+. Experimental parameters: photon energy 2.54 eV, laser power 10 µW, bath temperature 10 K. Scale bar is 5 µm. b) Room temperature PC map with a laser excitation of 850 nm (1.46 eV) with marked positions PC^0, PC^*, and PC^+. Scale bar is 5 µm. Four situations are highlighted.

(i) One position where there is a clear photocurrent maximum (PC* in S7b), while the photoluminescence is negligible (PL^0 in S7a).

(ii) One position where there is a clear photoluminescence maximum (PL* in S7a), while the photocurrent signal is negligible (PC^0 in S7b).

(iii) One position where both the photoluminescence and photocurrent maps show a maximum for the 2L-section (PL^+ and PC^+ in S7a,b).

(iv) The positions circle and cross, as already indicated in Fig. 1b,c in the main manuscript, show equivalently a maximum both in PL and PC, but for the 5L-section. The particular spectra are shown in Fig. 2 of the main manuscript.

The situations (i) and (ii) suggest that the charge carriers, as photogenerated within a local defect either tunnel across the hBN barrier (i) or recombine (ii). The cases (iii) and (iv) point towards the possibility that the tunneling and recombination rates can be balanced or that more than one defect is generated within the investigated position. The later possibility was revealed and discussed in great detail in reference [17] of the main manuscript. Note, the triangle indicates the position for the data in Fig. 4 of the main manuscript.

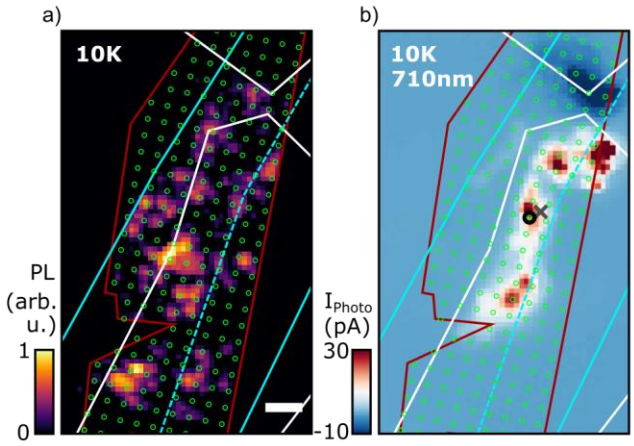

Figure S8: Low-temperature photoluminescence and photocurrent map. a) Photoluminescence map of the measured heterostack at a laser excitation of 530 nm (2.34 eV) and excitation power of 10 µW. Scale bar is 5 µm. b) Photocurrent map of the heterostack at a laser excitation of 710 nm (1.75 eV) and excitation of 80 µW. The bath temperature was 10 K.

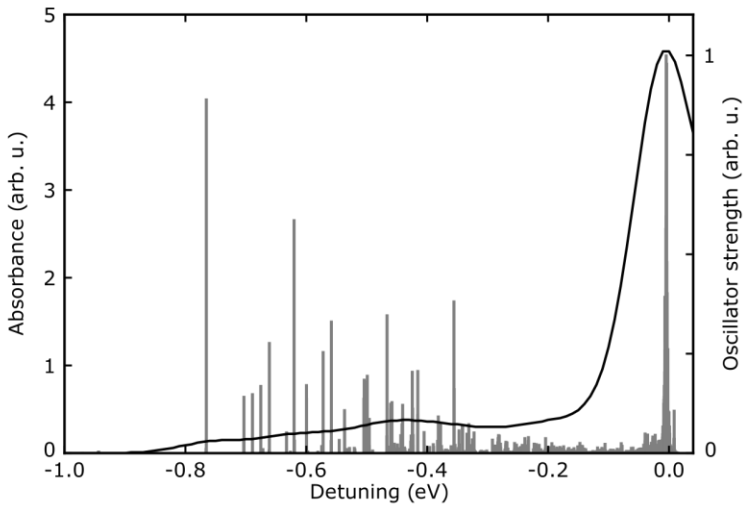

Figure S9: Calculated absorbance spectrum with discrete exciton energies. Calculated GW-BSE absorbance of monolayer MoS_2 with sulfur vacancies. For the calculation, we use a 5x5 supercell. The gray bars mark the oscillator strength (right axis) of the various excitons composing the continuous spectrum.